Fabric development with nearest-neighbor interaction and dynamic recrystallization

Throstur Thorsteinsson
Department of Earth and Space Sciences, University of Washington, Seattle, Washington, USA

Received 8 September 2000; revised 11 July 2001; accepted 11 July 2001; published 19 January 2002.

[1] Polycrystals undergoing ductile deformation develop lattice-preferred orientation (fabric) as a result of intracrystalline slip. A consequence of fabric development is that bulk physical properties become anisotropic. Fabric development and macroscopic deformation are studied by examining three effects: nearest-neighbor interaction (NNI) among crystals, polygonization, and migration recrystallization. The effects of NNI are modeled by arranging the crystals on a three-dimensional cubic grid and assigning six neighbors to each crystal. The "strength" of interaction can vary from no interaction (homogeneous stress) to "strong" interaction (significant stress redistribution). Increasing the NNI leads to a more homogeneous strain. Fabric varies in both strength and symmetry at a given bulk strain, depending on the strength of NNI. For a prescribed fabric the strain rate increases as the NNI increases. Recrystallization is modeled from energy balance considerations, and polygonization is formulated in terms of stress differences. Both processes require knowledge of dislocation density, which is calculated in the model as a function of crystal strain and grain size, both of which vary with time. Models of fabric development in ice that include NNI lead to more realistic fabric evolution than models with homogeneous stress. However, available data on fabric evolution are inadequate to determine quantitatively the strength of NNI acting in ice. *INDEX TERMS:* 1827 Hydrology: Glaciology (1863), 3210 Mathematical Geophysics: Modeling, 3902 Mineral Physics: Creep and deformation, 5120 Physical Properties Of Rocks: Plasticity, diffusion, and creep; *KEYWORDS:* glaciology, recrystallization, fabric, anisotropy, deformation, ice

1. Introduction

[2] The ductile behavior of crystalline materials like rocks and glacier ice depends on mechanical properties of individual grains in the aggregate and on interactions between the grains. In addition, the grain structure can also evolve in response to deformation, thereby altering the mechanical properties. These coupled processes have very important effects on the physical properties of crystal aggregates of many common earth minerals. An initially isotropic polycrystal undergoing ductile deformation will develop lattice-preferred orientation (fabric) as a result of intracrystalline slip. The preferred orientation of mantle minerals, mainly olivine crystals, is known to cause seismic shear wave splitting in the crust and the upper mantle [*Savage*, 1999]. In ice sheets, fabric evolution has been well documented from extensive thin section measurements on ice cores [*Alley et al.*, 1995; *Gow et al.*, 1997; *Thorsteinsson et al.*, 1997] and from sonic logging in boreholes and on the ice cores themselves [*Kohnen and Gow*, 1979; *Taylor*, 1982; *Anandakrishnan et al.*, 1994; *Thorsteinsson et al.*, 1999]. A consequence of fabric development is that bulk physical properties become anisotropic, as shown by experiments and theory [*Steinemann*, 1958; *Russell-Head and Budd*, 1979; *Duval*, 1981; *Duval and LeGac*, 1982; *Budd and Jacka*, 1989; *van der Veen and Whillans*, 1990; *Wenk and Christie*, 1991; *Alley*, 1992; *Anandakrishnan et al.*, 1994; *Azuma*, 1994, 1995; *Azuma and Goto-Azuma*, 1996; *Castelnau et al.*, 1996a].

[3] Several hypotheses have been used to model fabric development; the best known are the Taylor-Bishop-Hill (TBH), viscoplastic self-consistent (VPSC), and Sachs hypotheses. In the TBH hypothesis the key assumption is that all the crystals in the aggregate experience the same amount of strain, which guarantees compatibility (no voids or overlaps form), but not stress equilibrium [*Bishop and Hill*, 1951]. To achieve arbitrary deformation for every crystal, a minimum of four to five independent slip systems are required [*Wenk and Christie*, 1991]. Models based on the TBH hypothesis have mainly been used for crystals such as calcite where the plastic anisotropy is not very strong, and many easy slip systems are available [*Wenk and Christie*, 1991]. The VPSC method compromises between compatibility and stress equilibrium. VPSC models commonly assume that the neighborhood of each crystal is replaced with a homogeneous equivalent medium (HEM), which has the average properties of the aggregate. The HEM can have an anisotropic rheology [*Lebensohn and Tome*, 1993, 1994; *Molinari et al.*, 1987], and the HEM can be defined to encompass any given volume around a given crystal [*Molinari et al.*, 1987; *Wenk et al.*, 1991]. The VPSC scheme is an iterative scheme, and as such, it is sometimes difficult to visualize the redistribution of stress and strain between crystals at each step. The VPSC method has been used to model peridotite, olivine, quartz, and ice, to name only a few [*Wenk et al.*, 1991; *Castelnau et al.*, 1996b]. Finally, there are models based on the *Sachs* [1928] hypothesis, more precisely the homogeneous stress assumption, where the stress state in each crystal is assumed to be the same. It guarantees full stress equilibrium but not strain compatibility. *Thorsteinsson et al.* [1999] used this model to examine the effect of anisotropy on the deformation of the borehole in the ice sheet at Dye 3, Greenland.

[4] According to the TBH hypothesis the crystals are fully constrained by their neighbors, in the VPSC hypothesis they are partially constrained through the HEM, and in the Sachs hypothesis they are unconstrained since the deformation of each crystal depends only on the applied stress. For the fabric development in the Sachs model, on the other hand, the rotations are calculated as if the crystal were constrained by neighbors [*Castelnau et al.*, 1996b].

0418-0227/02/2001JB000244$09.00

[5] During fabric development the nearest neighboring crystals adjacent to a crystal are expected to have important effects on the deformation of that crystal. By means of in situ observation of plane strain deformation of polycrystalline ice, *Azuma* [1995] found that the deformation of single crystals depended very strongly on the interaction with their neighbors. Azuma formulated a fabric evolution model that is partly based on these findings [*Azuma*, 1994, 1995; *Azuma and Goto-Azuma*, 1996]. *Sarma and Dawson* [1996] used finite element modeling of polycrystals and found that neighbor interactions were the main factor in determining the variation of the single-crystal strain at a given bulk equivalent strain.

[6] Dynamic recrystallization is an important mechanism in fabric development during deformation. For temperatures (T) close to the melting point ($T > -12°C$ for ice), migration recrystallization is active. The high temperature allows the nucleation of new, strain-free grains and the rapid migration of grain boundaries [*Duval and Castelnau*, 1995]. In studies of high-temperature ($-5°C$ to $0°C$) creep of ice, *Kamb* [1972] found that after only $\sim$0.04 shear strain, there was already strong evidence of recrystallization. Polygonization is another recrystallization process in which grains are effectively divided due to rearrangement of dislocations into subboundaries (dislocation walls). The effect on fabric development from this process is less significant since the orientation of the new crystal usually deviates by <5° from the parent crystal.

[7] The purpose of this paper is to present a new model for fabric development. The model modifies the homogeneous stress assumption by redistributing the stress through explicit nearest-neighbor interaction (NNI). If there is no NNI, the model reduces to a homogeneous stress model. The effects of nearest-neighbor interaction on the behavior of crystal aggregates are examined. Dynamic recrystallization, both migration recrystallization and polygonization, is considered. Migration recrystallization depends on the dislocation density and crystal size, both of which have to be taken into account.

[8] In order to model the fabric development for a given material, one has to know the initial orientation distribution, the slip system (s) normals (and Burgers vectors), and their respective effective "viscosities," $\eta^s = \dot{\gamma}_0^s / (\tau_0^s)^n$, where $\dot{\gamma}_0^s$ and τ^s are reference shear strain rate and shear stress, respectively, and n is the stress exponent (inverse of strain rate sensitivity; see equation (3)).

[9] Ice (I_h, hexagonal) is used as the model material. Ice I_h has only two independent easy slip systems, the basal plane (0001) [*Ashby and Duval*, 1985]. Good information about fabric and texture exists from recent ice core studies [*Thorsteinsson et al.*, 1997; *Gow et al.*, 1997]. Resistance to shear on other slip systems (prism $(10\bar{1}0)\langle 11\bar{2}0\rangle$ and pyramidal $(11\bar{2}2)\langle\overline{11}23\rangle$ is 20 times, or higher, than on the basal plane slip system [*Castelnau et al.*, 1997]. The fabric development is qualitatively known from thin section and sonic logging measurements. The c axes rotate toward the compression axis [*van der Veen and Whillans*, 1994; *Morland and Staroszczyk*, 1998; *Gödert and Hutter*, 1998; *Thorsteinsson*, 2001].

[10] In this paper I will use fabric to refer to the orientation distribution of slip system normals $\mathbf{n}$ ($\langle 0001\rangle$ axes) and texture to refer to the size and shape of crystals.

2. The Model

[11] In the model the crystals are arranged on a three-dimensional cubic grid. Each crystal then has six nearest neighbors, as illustrated in Figure 1. The cubic arrangement is used to find nearest neighbors at all stages of the deformation. In this section I begin by writing the constitutive equation for a single crystal and explaining how the nearest-neighbor interaction (NNI) is taken into account. The bulk (macroscopic) deformation and crystal rotations are then derived. Finally, I describe how recrystallization (normal grain growth, polygonization, and migration recrystallization) is included in the model. Since the recrystallization depends on the dislocation density, an evolution equation for the dislocation density is also a part of the model.

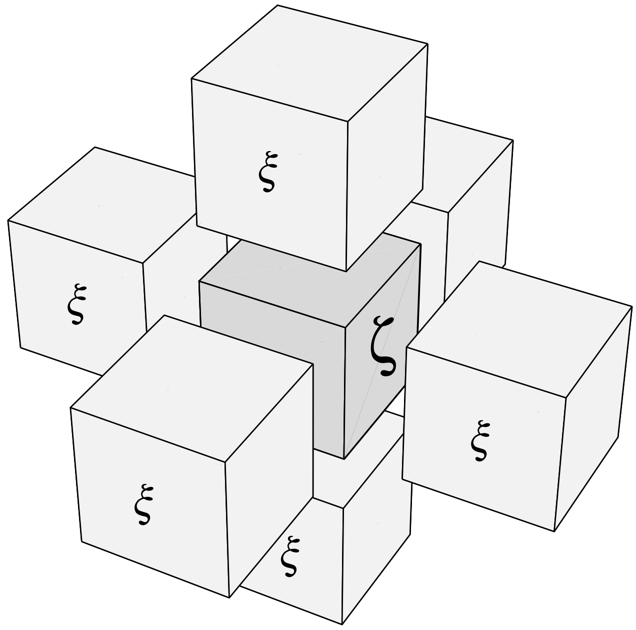

Figure 1. Illustration of the crystal arrangement used in the calculations. The center crystal is ζ, and its six nearest neighbors are ξ.

2.1. Constitutive Relations

[12] The resolved shear stress (RSS) on each slip system s is

$$\tau^s = \mathbf{S}^s : \mathbf{\Sigma}^c, \tag{1}$$

where $\mathbf{S}^s : \mathbf{\Sigma}^c = S_{kl}^s \Sigma_{kl}^c$ summing over repeated indexes, $\mathbf{\Sigma}^c$ is the state of stress in the crystal, and $\mathbf{S}^s$ is the Schmid tensor for the slip system. The Schmid tensor gives the transformation from the crystal coordinate system (microscopic) to the laboratory coordinate system (fixed, macroscopic)

$$\mathbf{S} = \mathbf{b} \otimes \mathbf{n}, \tag{2}$$

where $\mathbf{b} \otimes \mathbf{n} = b_i n_j$, $\mathbf{n}$ is the slip plane normal, and $\mathbf{b}$ is the slip direction (Burgers vector).

[13] The rate of shearing $\dot{\gamma}^s$, on slip system s, is

$$\frac{\dot{\gamma}^s}{\dot{\gamma}_0^s} = \left|\frac{\tau^s}{\tau_0^s}\right|^{n-1} \frac{\tau^s}{\tau_0^s}, \tag{3}$$

where $\dot{\gamma}_0^s$ and τ_0^s are the reference resolved shear strain rate and shear stress, respectively, and n is the stress exponent.

[14] The nearest-neighbor interaction (NNI) is modeled by defining a local softness parameter $\mathcal{E}$ for each crystal. The stress acting on the center crystal (Σ^c) is modified by $\mathcal{E}^c$ according to

$$\mathbf{\Sigma}^c = \mathcal{E}^c \boldsymbol{\sigma}, \tag{4}$$

where $\boldsymbol{\sigma}$ is the Cauchy stress tensor acting on the crystal aggregate. The softness $\mathcal{E}$ depends on the assigned strength of interaction, defined by the contribution of the center crystal (ζ) and the neighbors (ξ) to $\mathcal{E}$, and on the magnitudes of the resolved shear stress (RSS) of the neighbors compared to the center crystal. The contributions (ζ, ξ) thus determine the strength of interaction, and the magnitudes of the RSS of the neighbors determine the softness. The magnitude of the RSS is

$$\mathcal{T}^i = \left|\sum_s \tau^s \hat{\mathbf{b}}^s\right| = \left|\sum_s (\mathbf{S}^s : \boldsymbol{\sigma})\hat{\mathbf{b}}^s\right|, \tag{5}$$

where $\hat{\mathbf{b}}^s$ is a unit vector in the direction of the Burgers vector and $i = 0,1,\ldots, 6$ refers to the the center crystal and its six nearest neighbors. The local softness parameter $\mathcal{E}^c$ of each crystal is calculated from the ratio of $\mathcal{T}^0$ of the center crystal, relative to $\mathcal{T}^i$ of its neighboring crystals, and the relative contribution assigned to the neighbor crystals

$$\mathcal{E}^c = \frac{1}{\zeta + 6\xi}\left(\zeta + \xi\sum_{i=1}^{6}\frac{\mathcal{T}^i}{\mathcal{T}^0}\right), \tag{6}$$

where ζ is the contribution of the center crystal and ξ is the contribution of each neighbor, and since the RSS can be zero, there is a specified roof for the maximum value of $\mathcal{E}$.

[15] Setting $\zeta = 1$ and $\xi = 0$ in (6) gives $\mathcal{E} = 1$, which is the homogeneous stress model, where there is no neighbor interaction. When $\zeta = 6$ and $\xi = 1$, the center crystal contributes as much as all the neighbors together, while for $\zeta = 1$ and $\xi = 1$ the center crystal contributes as much as each of the neighbors. The effects of varying ζ and ξ are explored below.

[16] The strain rate is defined by $\dot{\varepsilon} = \frac{1}{2}\left(\mathbf{L} + \mathbf{L}^T\right)$, where $\mathbf{L}$ is the velocity gradient and superscript T denotes a transpose. The velocity gradient for a single crystal is related to the microscopic slip system shear strain rates by

$$\mathbf{L}^c = \sum_s \mathbf{S}^s\dot{\gamma}^s. \tag{7}$$

[17] Equations (3) and (7) show that the velocity gradient of a single crystal is

$$\mathbf{L}^c = \sum_s \dot{\gamma}_0^s \mathbf{S}^s \left|\mathcal{E}^c\frac{\mathbf{S}^s : \boldsymbol{\sigma}}{\tau_0^s}\right|^{n-1}\mathcal{E}^c\frac{\mathbf{S}^s : \boldsymbol{\sigma}}{\tau_0^s}, \tag{8}$$

where $\mathbf{S}$ is the Schmid tensor. The modeled velocity gradient of the aggregate is

$$\mathbf{L}^m = \frac{1}{N}\sum_{c=1}^{N}\mathbf{L}^c. \tag{9}$$

2.2. Rotation of Single Crystals

[18] To calculate the fabric development, the rotation of crystals with respect to the external reference frame must be formulated. A boundary condition of a bulk rotation rate $\dot{\boldsymbol{\Omega}}^b$ is imposed. The bulk velocity gradient is thus $\mathbf{L} = \mathbf{L}^m + \dot{\boldsymbol{\Omega}}^d$ [*Castelnau and Duval*, 1994] where

$$\dot{\boldsymbol{\Omega}}^d = \dot{\boldsymbol{\Omega}}^b - \dot{\boldsymbol{\Omega}}^m, \tag{10}$$

is the difference between the imposed bulk rotation $\dot{\boldsymbol{\Omega}}^b$ and the modeled rotation rate of the crystal aggregate

$$\dot{\boldsymbol{\Omega}}^m = \frac{1}{2}\left[\mathbf{L}^m - (\mathbf{L}^m)^T\right]. \tag{11}$$

[19] The rotation rate of the crystal lattice is given by

$$\dot{\boldsymbol{\Omega}}^* = \dot{\boldsymbol{\Omega}}^b - \dot{\boldsymbol{\Omega}}^p, \tag{12}$$

where $\dot{\boldsymbol{\Omega}}^b$ is the bulk (macroscopic) rotation rate and $\dot{\boldsymbol{\Omega}}^p$ is the plastic rotation rate of a single crystal

$$\dot{\boldsymbol{\Omega}}^p = \frac{1}{2}\left[\mathbf{L}^c - (\mathbf{L}^c)^T\right]. \tag{13}$$

The rate of change in orientation of $\mathbf{n}$ is given by

$$\dot{\mathbf{n}} = \dot{\boldsymbol{\Omega}}^* \cdot \mathbf{n}. \tag{14}$$

In the model calculations below, the change in the zenith and azimuth angle of the normal ($\mathbf{n}$) is calculated for each crystal. This also allows us to update the orientation of the three Burgers vectors in the basal plane [*Thorsteinsson*, 2001].

2.3. Dynamic Recrystallization

[20] For most polycrystalline materials, there are at least three recrystallization regimes: normal grain growth, polygonization, and migration recrystallization. The fabric (crystal orientation pattern) is not affected by normal grain growth, where grain size increases according to a parabolic growth law [*Gow*, 1971; *Alley et al.*, 1986]. As the grains strain, subboundaries (dislocation walls) may form due to heterogeneous deformation within grains that relieves stress concentrations. The formation of subboundaries can lead to the division of the parent grain into two new grains, as the misorientation of subgrains increases. This is called polygonization, and it leads to the formation of two grains with a small misorientation angle ($\sim$5°).

[21] The formation of subboundaries, by dislocations forming dislocation walls, can create small (fraction of parent crystal size) grains that are in a strain shadow. Being strain energy free, these small grains can act as seeds for migration recrystallization. The idea adopted here is that within the crystal aggregate, there are many such seeds. They are not explicitly formulated in the model since they are too small to contribute significantly to the deformation. However, they are envisioned to provide numerous potential nucleation sites for new grains. When the temperature gets high enough for grain boundary migration to be very efficient, these seeds can quickly consume highly strained crystals, thus reducing the free energy of the system. These small grains in the aggregate are also envisioned to allow for grain growth; larger adjacent grains can grow by consuming them.

[22] The number of crystals is kept constant in the calculations, so the volume (mass) can change discontinuously during recrystallization when new crystals replace old ones of different size. Only one of the two crystals resulting from polygonization is kept in the calculation; the choice is random. Since the orientations of the two parts are similar, this assumption does not significantly affect the NNI or the fabric. The change in both number and size of crystals would have to be taken into account for accurate modeling of texture (size and shape of grains). During migration recrystallization the new crystal is smaller (possibly equal in size) than the parent crystal, and the "missing mass" becomes "seeds," which are assumed to be present but are not explicitly included in the calculations. Polycrystalline ice is used as the model material, since good information about the transition between these recrystallization regimes exists from ice core studies.

2.3.1. Grain growth. [23] During normal grain growth the mean crystal diameter increases with time [*Gow*, 1971; *Alley et al.*, 1986] according to a parabolic growth law

$$D^2 - D_0^2 = Kt, \tag{15}$$

where t is time and D_0 is the mean crystal diameter at t = 0. The grain growth factor is

$$K = K_0 \exp\left(-\frac{Q}{RT}\right), \tag{16}$$

where T is the temperature, Q is activation energy, and K_0 is a constant that depends on impurity concentration. In the calculations below, $K_0 = 8.2 \times 10^{-9}$ m^2 s^{-1}, and Q = 40 kJ mol^{-1} is used to represent ice [*Alley et al.*, 1986].

[24] I have also used the difference in stored energy due to dislocations E_{disl} (see equation (19) below) to calculate the rate of change in individual crystal size [*Wenk et al.*, 1997] by changing the growth factor to

$$\tilde{K} = \left(E^{av}_{disl} - E^{i}_{disl}\right)K', \tag{17}$$

where E^{i}_{disl} is the stored energy of the crystal, E^{av}_{disl} is the average stored energy for the whole sample, and K' is a constant that depends on temperature and impurities. This allows some crystals to grow (if $E^{av}_{\mathrm{disl}} > E^{i}_{\mathrm{disl}}$) and others to contract ($E^{av}_{\mathrm{disl}} < E^{i}_{\mathrm{disl}}$).

2.3.2. Polygonization. [25] In the Greenland Ice Core Project (GRIP) ice core from the Greenland ice sheet, poly gonization (rotation recrystallization) is active below 650 m depth, where the vertical strain is ~0.25 [*Thorsteinsson et al.*, 1997]. *De La Chapelle et al.* [1998] found a lower bound for the dislocation density associated with the formation of a grain boundary by considering the energy associated with a dislocation density ρ and the energy corresponding to the formation of a grain boundary. They estimated that the dislocation density needed to form a wall is greater than $\rho_{\mathrm{poly}} \sim 5.4 \times 10^{10}$ m^{-2}.

[26] Here polygonization is modeled by considering a proxy for bending moments. Grains that have low RSS are likely to experience different stress from their neighboring grains, which are deforming. These stresses apply bending moments, which are relieved when the dislocations organize themselves into walls (subboundaries), effectively dividing the crystal [*Duval and Castelnau*, 1995]. To account for polygonization in the model, the magnitude of the RSS of the crystal is compared to the magnitude of the applied stress. If that ratio is smaller than a given value δ and if the dislocation density $\rho > \rho_{\mathrm{poly}}$, then the crystal polygonizes. The orientation is changed by $\Delta\theta$, the crystal size is halved, and the dislocation density ρ is reduced by ρ_{poly}. It is important to remember that grains rotate into a orientation with lower RSS as a result of intracrystalline slip. Some of the grains that have low RSS therefore have very high dislocation densities. Also, through the effects of NNI, a grain in a ''soft'' orientation can have a lower RSS if surrounded by ''hard'' grains. Typical values used below to model ice are δ = 0.065 and $\Delta\theta = 5°$.

2.3.3. Migration recrystallization. [27] Migration recrystallization is generally active when the temperature is close to the melting point. In ice it is active when the temperature exceeds ~−12°C, but for colder temperatures it is generally not observed [*Duval and Castelnau*, 1995]. To model migration recrystallization, both stored energy and energy associated with grain boundaries must be considered. The energy associated with grain boundaries is

$$E_{gb} = \frac{3\gamma_{gb}}{D}, \tag{18}$$

where γ_{gb} = 0.065 J m^{-2} (for high angle boundaries) and D is the crystal diameter. The stored energy due to a dislocation density ρ can be estimated as

$$E_{\mathrm{disl}} \simeq \kappa\rho G b^2 \ln\frac{R_e}{b}, \tag{19}$$

where G is the shear modulus, b is the length of the Burgers vector, κ is $(4\pi)^{-1}$ for screw and $[4\pi(1-\nu)]^{-1}$ for edge dislocations (where $\nu \simeq 0.3$ is the Poisson's ratio), and R_e is the mean average of the dislocation strain field range [*Mohamed and Bacroix*, 2000; *Kuhlmann-Wilsdorf*, 1998, 1999]. R_e is commonly approximated by $1/\sqrt{\rho}$, but *Mohamed and Bacroix* [2000] found that this leads to an underestimate of E_{disl}; κ is therefore treated as an adjustable parameter, but R_e is kept as $R_e = 1/\sqrt{\rho}$. For ice, $G \simeq 3.4 \times 10^9$ Pa and $b = 4.5 \times 10^{-10}$ m.

[28] Migration recrystallization is included in the model by considering the balance between the stored energy E_{disl} associated with the dislocation density and the grain boundary energy E_{gb}. As the crystals strain, the dislocation density increases, and it becomes energetically favorable to recrystallize if the energy due to the dislocation density (E_{disl}) exceeds the grain boundary energy E_{gb} that is created by the recrystallization. Tracking of both the crystal size and dislocation density is therefore needed. An estimate of the change in dislocation density ρ with time is given by

$$\frac{\partial\rho}{\partial t} = \frac{\dot{\varepsilon}}{bD} - \alpha\rho\frac{K}{D^2}, \tag{20}$$

where α is a constant >1, K is the grain growth factor, and D is the crystal diameter [*De La Chapelle et al.*, 1998; *Montagnat and Duval*, 2000]. The first term on the right-hand side represents the increased dislocation density, by work hardening, and the second term represents the absorption of dislocations at grain boundaries (recovery). Although the details of the processes at the grain level are more complicated than formulated in (20) [*Miguel et al.*, 2001], these two processes are the most significant.

[29] In the model the crystal size D and dislocation density ρ are calculated at each step. When $E_{\mathrm{disl}} > E_{gb}$, the crystal recrystallizes. The crystal is then replaced with a new ''strain-free'' crystal, with dislocation density $\rho_0 = 10^{10}$ m^{-2} [*Montagnat and Duval*, 2000]. The size of the new crystal scales with the effective stress $\sigma_e^2 = \sigma_{kl}\sigma_{kl}/2$ as $D_0 \sim \sigma_e^{-1.33}$ [*Guillope and Poirier*, 1979; *Ross et al.*, 1980; *Shimizu*, 1998, 1999]. A totally random orientation for the new grain is not to be expected; some subset of possible zenith angles seems more likely. In uniaxial compression of ice, for instance, a small circle girdle fabric forms [*Budd and Jacka*, 1989]. This indicates that new crystals that form in orientations with high RSS are favored to grow. The orientation of the new crystal is chosen at random from within a specified range of possible angles in the model. This range corresponds to the ''softest'' orientations in the applied stress state. In uniaxial compression, for example, the range within which new crystals can form is chosen to be between 35° and 55°.

3. Model Results

[30] This section explores the effects of several levels of nearest-neighbor interaction (NNI) and recrystallization assumptions on the fabric development and bulk behavior. The results are then compared with data from the GRIP ice core.

[31] In the following, deformation by dislocation glide on the basal plane slip system is considered, using ice as the model material. *Kamb* [1961] showed that for the observed range of the stress exponent, $2 < n < 4$, the expected response to simultaneous glide along the a axes differs so slightly from the hitherto-postulated a axis-independent, noncrystallographic glide as to be practically undetectable experimentally. The resistance to slip on the basal plane is the same for the three a axes, and only the basal slip system is considered for ice; therefore we can write

$$\frac{\dot{\gamma}^s_0}{\left(\tau^s_0\right)^n} = \beta A(T), \tag{21}$$

where β is a constant, and $A(T) = A_0 \exp(-Q/RT)$, where A_0 is a constant, Q is the thermal activation energy, R is the gas constant,

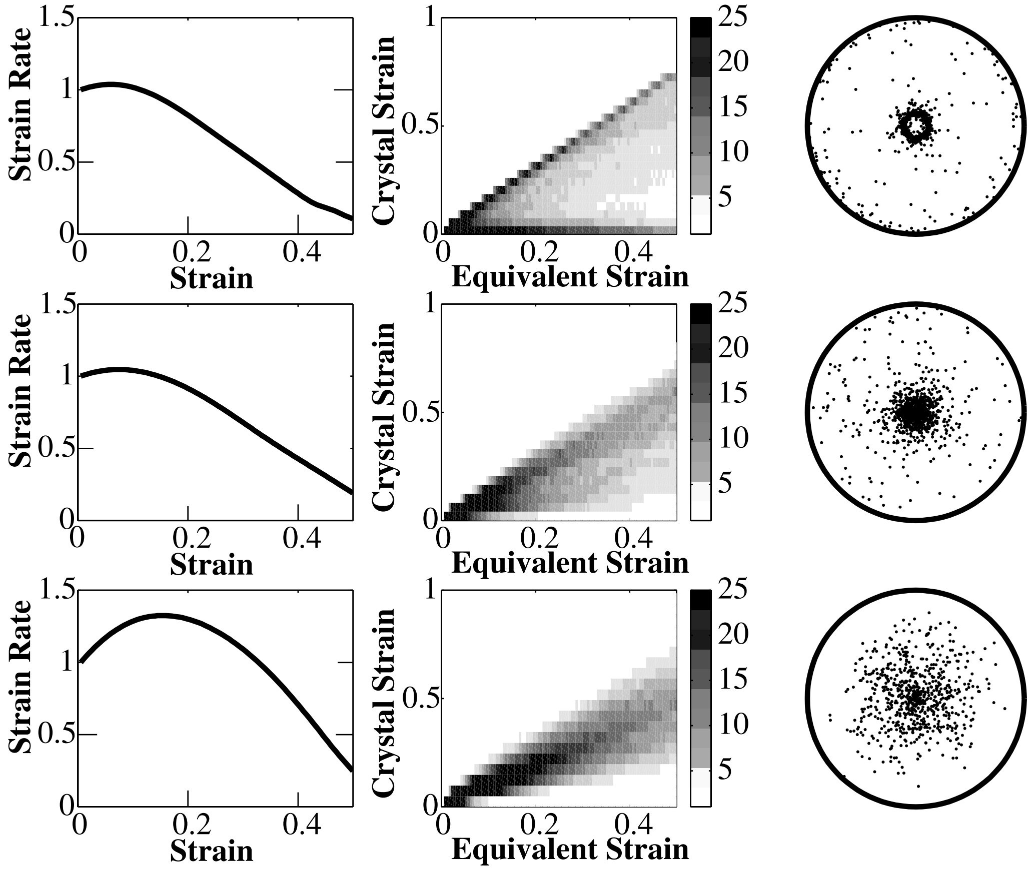

Figure 2. Model results for uniaxial compression deformation for varying NNI: (top) no-NNI (1,0), (middle) mild-NNI (6,1), and (bottom) full-NNI (1,1) cases. (left) The normalized vertical strain rate versus the vertical strain. (middle) The distribution of single-crystal strain as a function of bulk equivalent strain, where the scale bar shows the percentage of crystals with a given strain. (right) The final fabric achieved in each case.

and T is the temperature. The parameter β is chosen such that an isotropic distribution yields the same strain rates as *Glen*'s [1958] flow law, or some reliable measurements.

3.1. Nearest-Neighbor Interaction (NNI)

[32] The effects of the NNI on the fabric development are examined first without any recrystallization. Three types of NNI are used, $(\zeta, \xi) = (1,0)$, $(6,1)$ and $(1,1)$, which will be called the no-NNI, mild-NNI, and full-NNI cases, respectively.

[33] Figure 2 shows model results for ice deformed under constant uniaxial compressive stress along the 3 axis. Figure 3 shows the results for ice deformed in constant pure shear stress ($\sigma_{33} = -\sigma_{11}$). Each row shows the results for different NNI. The left plot in each row shows the strain rate, $\dot{\varepsilon}_{33}$, normalized by the initial isotropic strain rate, as a function of axial strain

$$\varepsilon_{33} = \sum_{i=1}^{N} \dot{\varepsilon}_{33}^{i} \Delta t_i,$$

where Δt_i is the time it takes to complete the strain step i and N is the number of steps. The middle plot in each row shows the strain of single crystals as a function of the bulk equivalent strain, $\varepsilon_{eq} = \sum_{i=1}^{N} \dot{\varepsilon}_{eq}^{i} \Delta t_i$, where

$$\dot{\varepsilon}_{eq} = \sqrt{\frac{2}{3} \dot{\varepsilon} : \dot{\varepsilon}}.$$

The results are displayed as a density plot, where the percentage of crystals within a given strain (range) at a given bulk strain (range) is shown. The right plot in each row is the resulting fabric at the end of the model run.

[34] In the uniaxial compression model run (Figure 2) the maximum strain rate generally increases with increasing NNI. In pure shear (Figure 3), that effect is very small, since the fabric evolution is less favorable for the deformation; the fabric locks up. The strain of individual crystals with no NNI in uniaxial compression follows two primary branches, zero strain or rapid strain. Many of the crystals are simply not deforming. With increasing NNI the spread diminishes, and for full NNI all the crystals deform to some extent. The final fabric shows that NNI induces a distinct change in character of the final fabric; compare the top and bottom row of Figures 2 and 3. Increasing NNI tends to increase the spread of crystal orientations, since the "hard" crystals are now deforming. Similar observations apply to the pure shear deformation.

[35] It is clear from the final fabric in Figure 2 that the rate of change of the zenith angle θ (zenith angle velocity, $d\theta/dt$) changes as the NNI changes. Figure 4 shows the zenith angle velocity for the no-NNI, mild-NNI, and full-NNI cases. When there is no NNI, the zenith angle velocity of each crystal at a given zenith angle is a constant. When there is NNI, the zenith angle velocity at a given zenith angle depends on the nearest neighbors. The mean velocity at a given zenith angle is thus different from the no-NNI case. From Figure 2 we see that the maximum zenith angle velocity, of

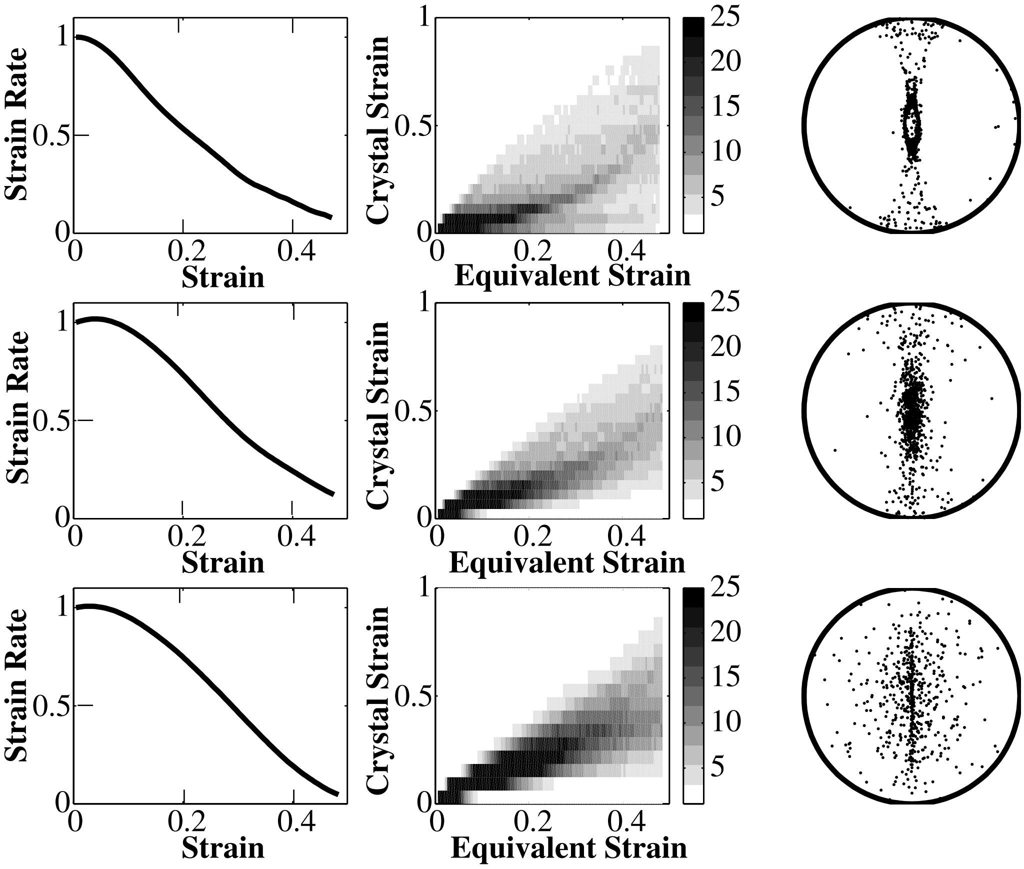

Figure 3. Model results for pure shear stress state deformation for varying NNI: (top) no-NNI (1,0), (middle) mild-NNI (6,1), (bottom) full-NNI (1,1) cases. (left) The normalized vertical strain rate versus the vertical strain. (middle) The distribution of single-crystal strain as a function of bulk equivalent strain, where the scale bar shows the percentage of crystals with a given strain. (right) The final fabric achieved in each case.

the bulk average, decreases as the interaction increases but the velocity is more uniform over a range of zenith angles.

3.2. Dynamic Recrystallization

[36] In the following, the model starts with an initial fabric which has a random distribution of *c* axes (isotropic ice), randomly assigned crystal size of 3 to 5 mm diameter with a mean of 4 mm, and a constant dislocation density of $\rho = 4 \times 10^{10}$ m^{-2} for each crystal. The stress level is ~0.1 bar, and in the examples below, the crystal size remained essentially constant because only a short time was required to achieve the strain.

[37] The results in uniaxial compression with mild NNI and polygonization are shown in Figure 5. The strain rate versus strain, the single-crystal strain density, and the final fabric are shown in Figure 5 (top), and the polygonization events are shown in Figure 5 (bottom). The temperature is too low for migration recrystallization to be active. Polygonization starts at a vertical strain of ~0.03. The minimum dislocation density needed to form subboundaries is $\rho_{poly} = 5.4 \times 10^{10}$ m^{-2}. If the magnitude of the RSS for a crystal is <6.5% of the applied stress magnitude, and if the dislocation density is high enough, then the crystal can polygonize. This process is represented by setting $\delta = 0.065$. Each time a crystal polygonizes, the dislocation density is reduced by ρ_{poly}. The zenith angle changes by ±5°; if the crystal is within 30° of vertical, the sign is positive (crystal moves away from vertical); otherwise, the sign is chosen at random. The strain rate is higher than in the case without polygonization, since crystals in "hard" orientations are preferentially removed by the polygonization criteria. The single-crystal strain distribution is more homogeneous at a given bulk equivalent strain, and the final fabric is not as strong (compare with the middle row of Figure 2).

[38] Figure 6 shows the results when migration recrystallization is active. The strain rate versus strain, the single-crystal strain density, and the final fabric are shown in Figure 6 (top), and the recrystallization events are shown in Figure 6 (bottom). Initially, all the crystals have the same dislocation density $\rho = 4\rho_0$, so E_{disl} is very small relative to the grain boundary energy. However, as the crystals strain at different rates, the stored energy (E_{disl}) increases and in some crystals eventually reaches E_{gb}; crystal growth/contraction is negligible in these calculations. I used $\kappa = 0.35$ to simulate the steady tertiary creep of ice after ~10% strain; values of κ smaller than 0.2 did not result in strong girdle fabrics. Larger values of κ would initiate migration recrystallization for lower dislocation density, i.e., at lower strains, and results in stronger recrystallization "waves." When the stored energy of a crystal exceeds E_{gb}, that crystal will recrystallize. The first recrystallization event occurs after 0.005 equivalent strain, and ~4% of the crystals recrystallize at each step (0.001 equivalent strain) after the initial peak. The strain rate increases rapidly at first, but after ~0.1 strain it levels off, approaching normalized strain rate $\left(\dot{\varepsilon}/\dot{\varepsilon}_{isotropic}\right)$ of ~3. A similar pattern is observed in laboratory experiments [*Budd and Jacka*, 1989]. Individual grains acquire only ~0.03 strain before their E_{disl} exceeds the E_{gb}; the crystal size is ~4.2 mm throughout.

[39] Comparison of model results with measured fabric is complicated, especially since the initial fabric is often not truly random. At the GRIP borehole, Greenland, the fabric close to the surface does not have an isotropic orientation distribution. This is clearly demonstrated in Figure 7, showing the *c* axis orientations of

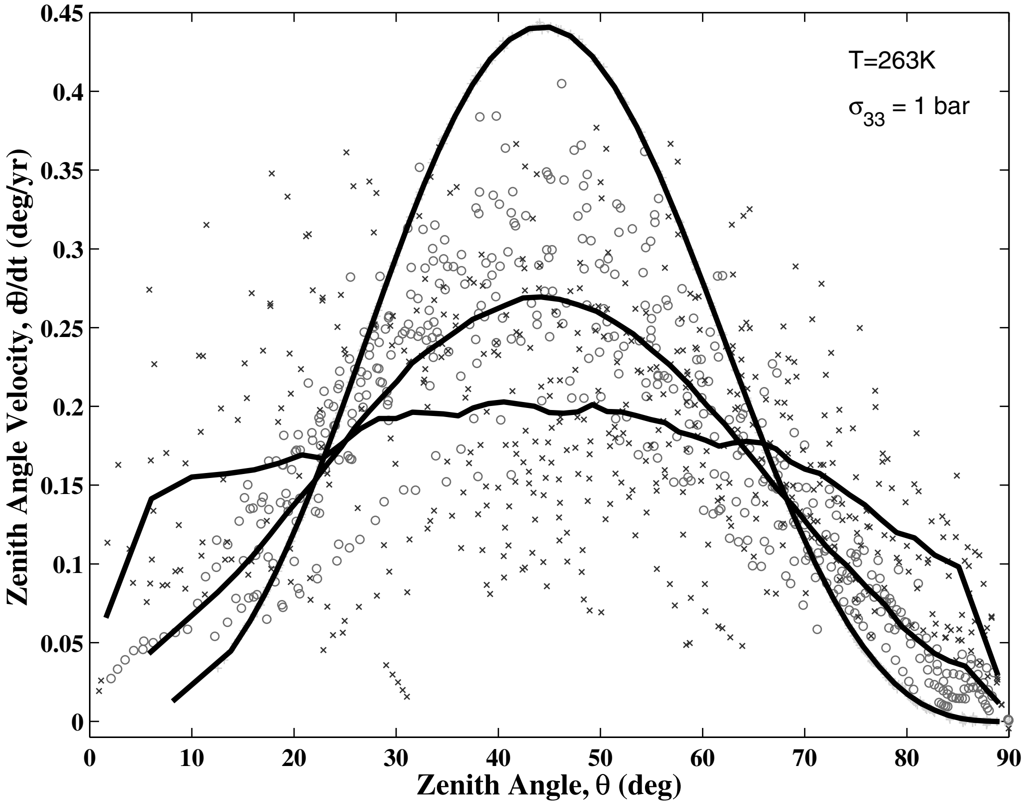

Figure 4. Zenith angle velocity, $d\theta/dt$, in uniaxial compression as a function of zenith angle θ for different levels of NNI. The pulses result from no-NNI (1,0), circles result from mild-NNI (6,1), and crosses result from full-NNI (1,1) cases. In each case a mean velocity curve is plotted, which uses the average over ~5° steps. Note that the pluses are almost completely hidden behind the curve for the no-NNI case. Only a few of the 50×10^3 data points for each level of NNI are shown here.

the ice at 139 m depth. The strain (<0.1) that the ice has experienced is insufficient to reorient the crystals significantly, yet the fabric is far from the sine curve distribution characteristic of isotropic ice.

[40] Keeping in mind the complications mentioned above, Figure 8 shows a comparison of the model results, using mild NNI with polygonization, with fabric data from the GRIP borehole, Greenland [*Thorsteinsson et al.*, 1997]. The vertical strain is ~0.25

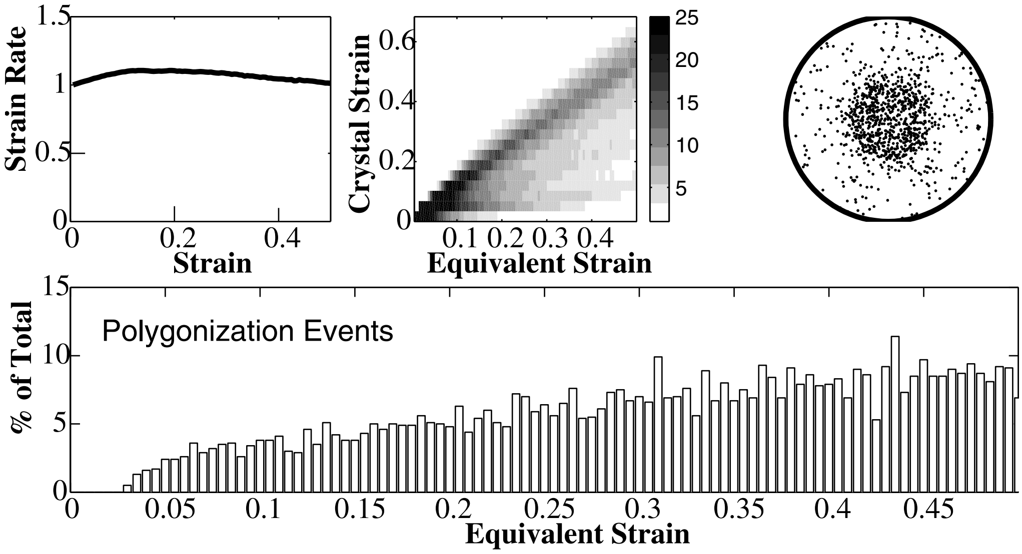

Figure 5. Results from uniaxial compression with mild NNI, (ζ, ξ) = (6,1), and polygonization (δ = 0.065). (top) The normalized strain rate versus axial strain, the strain density of single crystals, and the final fabric. (bottom) The polygonization events after each strain step as a percentage of the total number of crystals. Each step is equal to an equivalent strain of 0.005.

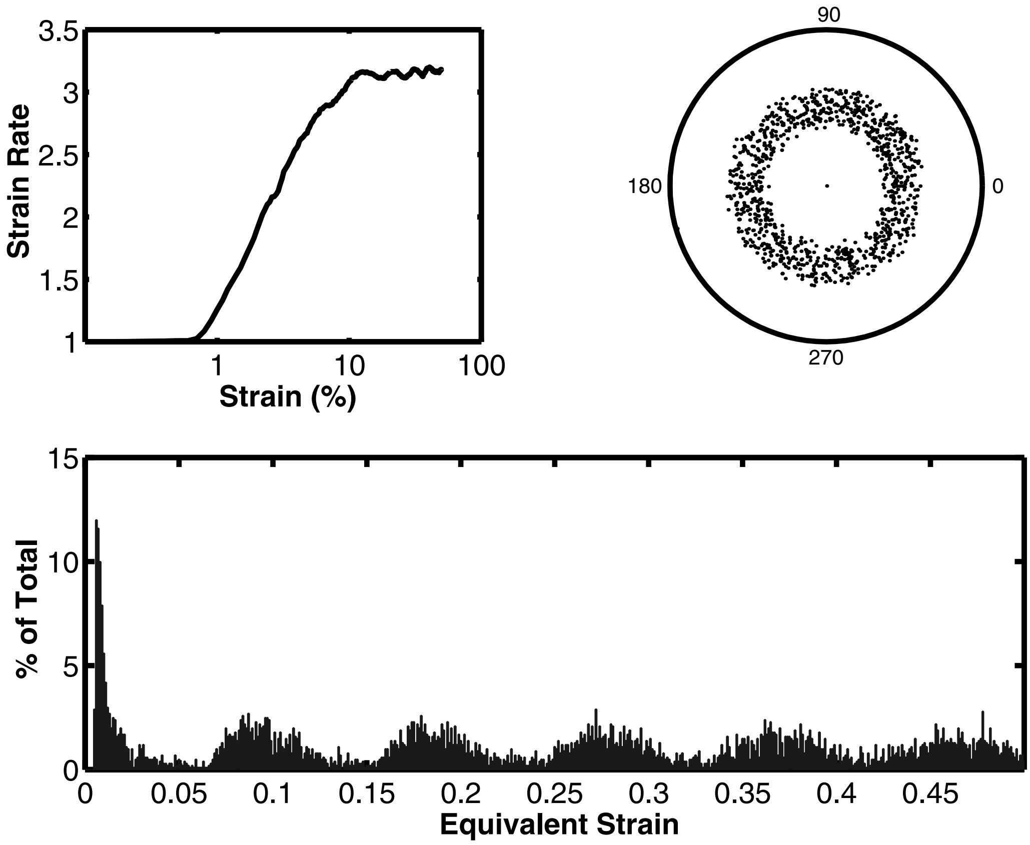

Figure 6. The normalized strain rate versus axial strain, final fabric, and recrystallization events for mild NNI in uniaxial compression with migration recrystallization. The recrystallization events are shown as the total number of crystals that recrystallized after each strain step of equivalent strain of 0.001.

at 650 m depth and ~0.5 at 1293 m depth. The initial fabric in the model was isotropic, and the criteria for polygonization are the same as above. The temperature is below −12°C so there is no migration recrystallization. The zenith angle averaging includes all 1000 crystals used in the model run. The results for mild NNI are in broad agreement with the measured fabric. Model runs with no interaction (no NNI) lead to a much stronger fabric and be ruled out. Full NNI produces fabric that is more evenly distributed than the mild-NNI fabric, but for samples of only a few hundred crystals the distributions do look very similar, and therefore full NNI cannot be ruled out.

3.3. Sensitivity to the Number of Crystals Used

[41] This model can be used to calculate the instantaneous deformation for a predescribed fabric. The question, then, is how many crystals are needed to represent the fabric for strain

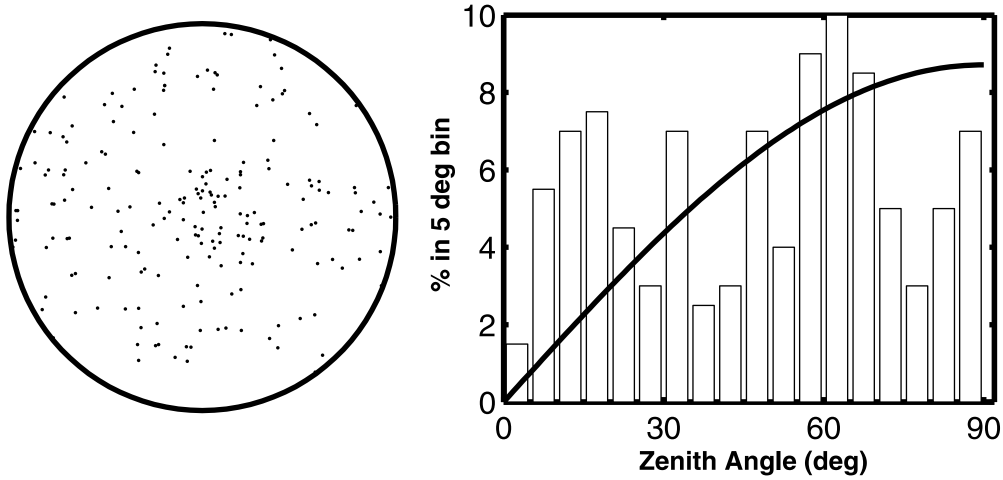

Figure 7. Fabric at 139 m depth in the GRIP bore-hole, Greenland [*Thorsteinsson et al.*, 1997]. The Schmidt plot shows the distribution of all the 200 crystal *c* axes, and the bar plot shows the number of crystals in 5° zenith angle bins. The distribution is far from the isotropic distribution shown by the solid line.

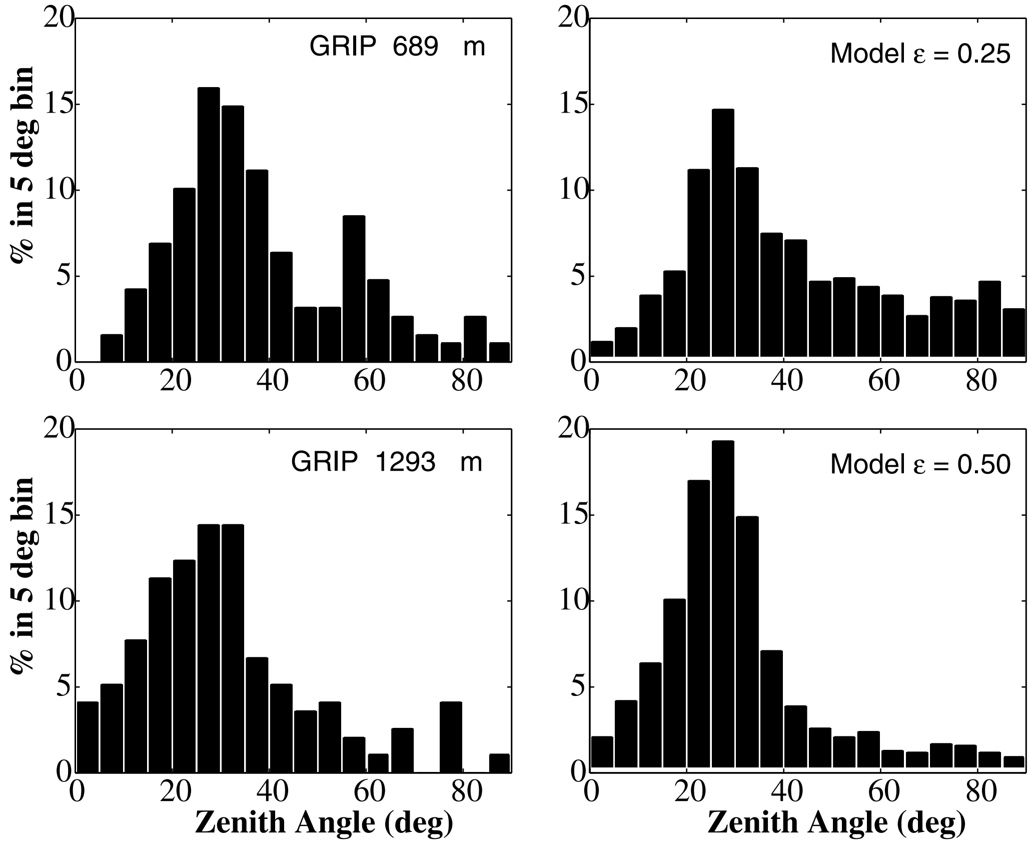

Figure 8. Comparison of the measured and calculated zenith angle distributions at two depths in the GRIP core. The measured fabric obtained from thin sections done on the grip ice core [*Thorsteinsson et al.*, 1997]. The zenith angles are binned in 5° bins (188 crystals at 689 m and 194 at 1293 m), and the same applies to the 1000 crystals from the model. (right) The model calculations made with mild NNI and δ = 0.065.

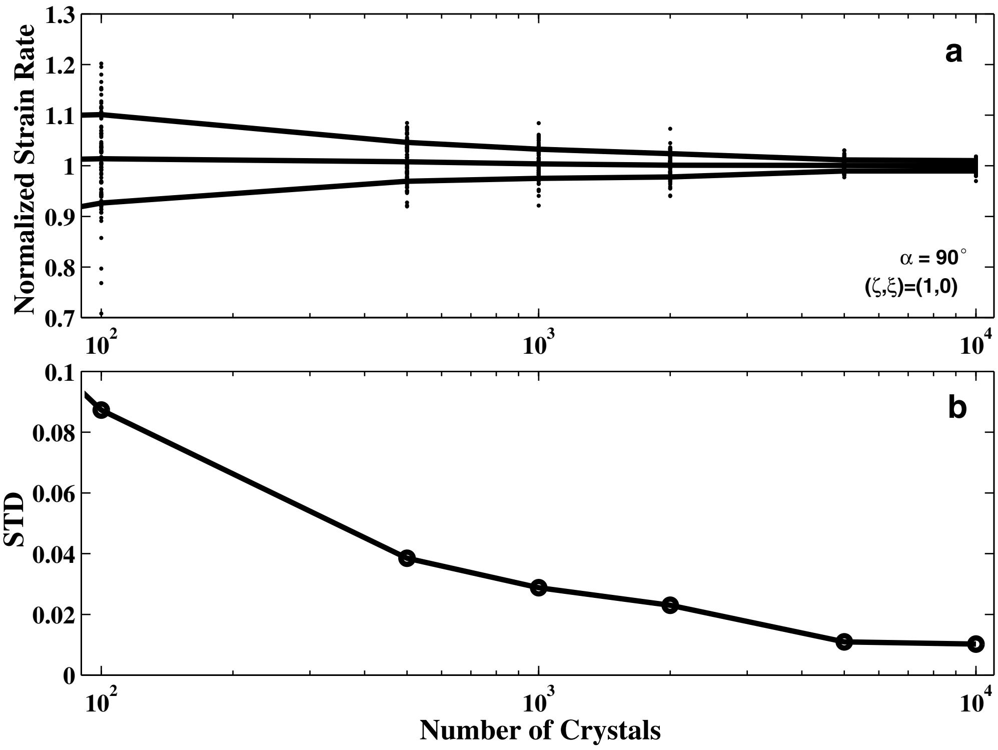

Figure 9. Examining the effect of the number of crystals used in the calculations (a) Normalized strain rate (calculated divided by theoretical) of an isotropic ice with no NNI as a function of the number of crystals used in the simulation. (b) The standard deviation of the normalized strain rates as a function of the number of crystals used.

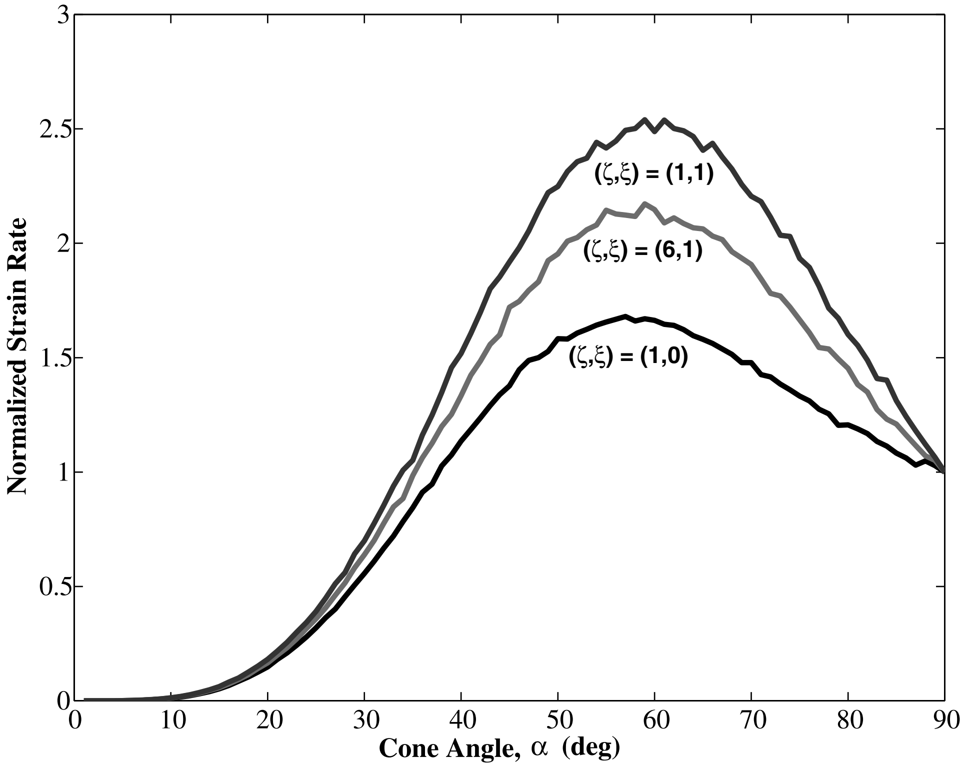

Figure 10. Normalized strain rates in uniaxial compression as a function of cone angle for no (1,0), mild (6,1), and full (1,1) nearest-neighbor interaction.

rate calculations? First, I examine how many crystals are needed to give an accurate description of isotropic ice. In the model the crystal orientations are chosen at random; an infinite number of crystals are needed to exactly satisfy isotropy. The calculations of strain rate must depend to some extent on the finite number of crystals used; obviously, 100 crystals chosen at random cannot uniformly cover the lower hemisphere. For each given number of crystals in Figure 9 the strain rate is calculated 100 times, each time using a new random fabric. Then the mean and standard deviation (SD) of the strain rates are calculated for the 100 numerical experiments. Since the correct strain rate for an infinite number of crystals is known analytically [*Thorsteinsson*, 2001], it can be used to normalize the resulting strain rates. Figure 9 shows how the number of crystals used in a calculation affects the accuracy. Note that the SD declines greatly as the number of crystals increases from 100 to ~5000. The improvement between 5000 and 10,000 crystals is minimal. I conclude that accurate results are achieved using a 20 × 20 × 20 arrangement of crystals.

[42] Note also that the ratio of the number of crystals at the surface of the cubic arrangement to the total number of crystals, $R_d = S/V = 4\,d^2/d^3 = 4/d$ goes from 40% for 10^3 crystals to 20% for 20^3 crystals. This is important since a periodic arrangement of crystal boxes is used for the NNI (that is, the arrangement shown in Figure 1 is repeated for 20^3 crystals in each box).

[43] Having established that ~8000 crystals can be used to adequately represent the strain rate, the strain rate as a function of fabric can now be modeled. An example fabric is a vertically orientated cone, which is described by a cone angle α, which is half the apex angle of the cone within which the crystals are evenly distributed. Figure 10 shows the normalized strain rate, $\dot{\varepsilon}_{33}(\alpha)/\dot{\varepsilon}_{33}(90^\circ)$, in uniaxial compression as a function of cone angle. With increasing interaction the maximum strain rate increases. Figure 11 shows how increasing NNI increases the maximum enhancement in a simple shear stress state.

4. Discussion

[44] In the model the level of stress for each crystal depends on the orientation of the crystal and the orientation of the nearest neighbors (except in the no-NNI case). The crystals are arranged on a cubic grid, and that arrangement does not change during the deformation. The formulation applies equally well to other crystal arrangements. The model could be extended to include next-to-nearest-neighbor interaction, which would presumably make a smaller contribution to the local softness. The nearest-neighbor interaction leads to more enhanced deformation rates for cone angles between 40° and 90° in uniaxial compression along the direction of the cone (Figure 2). The same is not true in pure shear (Figure 3) because the deformation quickly moves the crystals into unfavorable orientations, where the RSS is smaller.

[45] Fabric plots from various ice cores show that the crystals in uniaxial compression move toward and reach vertical, and few are left near horizontal. This indicates that some NNI is needed, since the zenith angle velocities for no NNI (Figure 4) go quickly to zero near horizontal and vertical, and therefore the crystal *c* axes in compression (Figure 2) do not reach vertical, nor do they move out of horizontal starting positions. The strength of NNI is difficult to constrain from available thin section data, since closely spaced thin sections often show very different fabric and generally contain only a few hundred crystal orientations.

[46] Since I keep track of grain size in the model, it would be possible to assign weight according to grain size. I did not do that here since the grain size that was used was fairly uniform and deformation of ice under the conditions modeled does not show a strong dependence on grain size [*Duval and LeGac*, 1980].

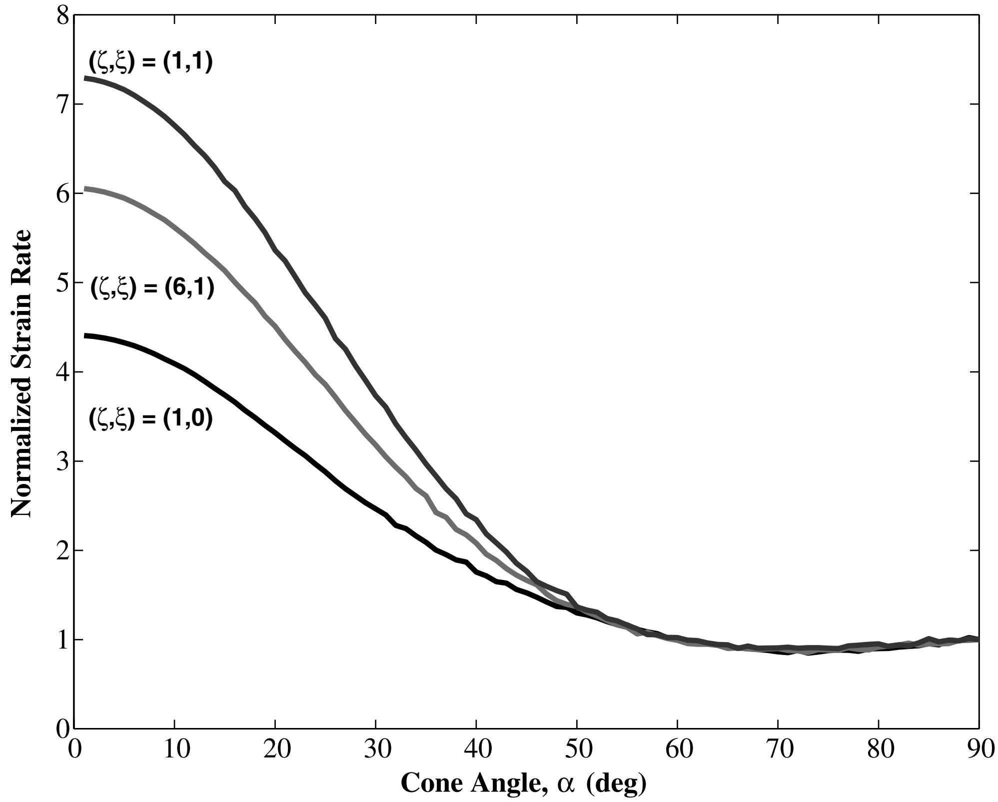

Figure 11. Normalized strain rates in simple shear stress as a function of cone angle for no (1,0), mild (6,1), and full (1,1) nearest-neighbor interaction.

However, grain size may be important when mechanisms other than intracrystalline slip contribute to the deformation [*Goldsby and Kohlstedt*, 1996; *Cuffey et al.*, 2000]. During grain growth, grains smaller than some critical size are being consumed. These grains also act as seeds for recrystallization. They can be pictured as tiny strain-free subgrains that do not contribute to the deformation because of their small size but can quickly consume highly strained adjacent grains. To model the grain size evolution accurately, a better model of the grain size statistics is needed. One particular future direction for modeling would be to let the total number of grains vary.

[47] The choice of the simple relation for grain growth (equation (15)) or the one dependent on the stored energy (equation (17)) does not change the results of the fabric evolution or strain history. When the stored energy E_{disl} (equation (19)) is used to calculate grain boundary migration rates [*Wenk et al.*, 1997], some grains grow, and others get smaller. However, to model grain size evolution realistically, consideration of differences in the stored energy between neighboring grains would be necessary to allow for inhomogeneous grain growth. Ice, for instance, often shows interlocking texture [e.g., *Duval and Castelnau*, 1995]; a simple expansion or contraction of each grain would not explain those observations.

[48] Polygonization takes place in the model when the grains are most likely to be affected by the inhomogeneity of the stress state at the grain size scale. This is achieved by comparing the magnitude of the RSS on the basal plane of the grain to the magnitude of the applied stress. If that ratio is low, it is likely that the grain experiences forces from deforming neighbors. Grains with higher RSS and high dislocation density can also form subboundaries (P. Duval, personal communication, 2000). This is partly accounted for by the fact that as the grains strain, they eventually rotate into orientations with low RSS and therefore can polygonize and by the fact that a grain surrounded by stiff grains has a lower RSS than if there were no NNI.

[49] Migration recrystallization is difficult to model. Very complex models of dislocation interactions and grain boundary migration are needed to incorporate the fundamental physics. The approach taken here is to parameterize this process by considering the energies involved. However, even the energy associated with a dislocation density ρ is difficult to estimate [*Mohamed and Bacroix*, 2000; *Kuhlmann-Wilsdorf*, 1998]. The resulting fabric and strain rate (Figure 6 using equation (19) with $\kappa = 0.35$) are very similar to laboratory measurements [cf. *Budd and Jacka*, 1989, Figure 8]. This value of κ is similar to suggested values for a mix of screw and edge dislocations, $\kappa = 0.1$ [*Mohamed and Bacroix*, 2000]. There is also considerable uncertainty about the orientation of newly recrystallized grains. For ice the girdle pattern obtained in Figure 6 is commonly observed [*Budd and Jacka*, 1989]. That clearly indicates that there is a preferred orientation for the newly formed grains, but whether it is due to oriented nucleation or oriented growth is uncertain [*Branger et al.*, 2000; *Rajmohan and Szpunar*, 2000]. The modeled strain rate prior to 1% strain will look different from experimental data since there is no initial redistribution of stress or an elastic response. For strain $\geq$1% the modeled and the measured strain rates are almost identical. However, since only the final orientations of $<$100 crystals are generally available from experiments, the trade-off between the effects of fabric and the NNI on the strain rate prevents determination of the strength of NNI.

[50] Figure 12 shows a comparison of the fabric modeled in uniaxial compression, after an axial strain of 0.5, using *Azuma*'s [1994] model, and the model described here with no NNI (homogeneous stress; Sachs model), mild NNI, and full NNI. For comparison, the fabric at 1293 m depth in the GRIP borehole is also shown [*Thorsteinsson et al.*, 1997], where the strain is $\sim$0.5 [*Castelnau et al.*, 1996b]. There is active polygonization at this

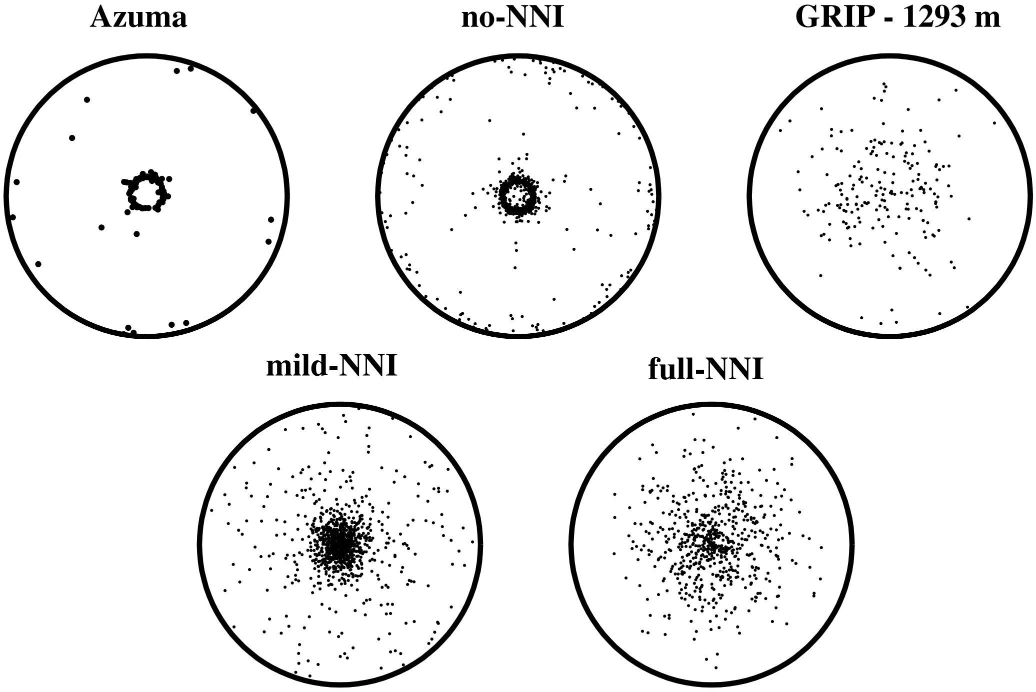

Figure 12. Comparison of modeled fabric in uniaxial compression, after 0.5 strain. *Azuma*'s [1994] model and the no-NNI version of the model described here predict fabric that evolves too quickly compared to the GRIP fabric. The mild-NNI and full-NNI cases are in much closer agreement. Note that the fabric plot for Azuma's model has 100 crystals, GRIP fabric has 194, and other plots have 1000 crystals.

depth in the GRIP core, but as we have seen, this does not significantly change the fabric. The fabrics predicted by the Azuma and Sachs model evolve too quickly. In ice sheets the fabric is much closer to the mild- and full-NNI cases; compare those to the GRIP fabric at 1293 m depth. The VPSC model yields fabrics that are very similar to the mild-NNI (VPSC spherical) and full-NNI (VPSC ellipsoidal) cases (for strain of 0.4)[*Castelnau et al.*, 1996a, Figure 8]. VPSC spherical refers to model runs where the crystals remain spherical throughout, and VPSC ellipsoidal refers to model runs where the shape is represented by an evolving ellipsoid [*Molinari et al.*, 1987]. Calculating the fabric evolution for 1000 crystals using 100 steps to reach 0.5 strain requires ~25 s of CPU time on a 450-MHz Pentium III workstation.

5. Conclusions

[51] The nearest-neighbor interaction (NNI) changes the overall pattern of fabric development. With increasing interaction the strain of single crystals becomes more evenly distributed; this changes the rate of fabric development. From comparison with measured fabric I conclude that some NNI is necessary, but the required interaction strength is difficult to assess. The recrystallization part of the model is able to yield realistic results, but more data on fabric (evolution) are needed to constrain the free parameters.

Notation

- $\mathbf{n}$ normal to slip plane ($\mathbf{c}$ in ice).
- $\mathbf{b}$ Burgers vector.
- s slip system.
- $\dot{\gamma}$ strain rate on a slip system [1/s].
- τ resolved shear stress on a slip system [Pa].
- $\dot{\varepsilon}$ strain rate [1/s].
- $\boldsymbol{\sigma}$ stress [Pa].
- $\boldsymbol{\Sigma}$ stress acting on crystal [Pa].
- $\mathbf{S}$ Schmid tensor.
- $\mathcal{E}$ local softness parameter.
- $\mathcal{T}$ magnitude of RSS.
- δ critical ratio of RSS and equivalent stress.
- ζ, ξ contribution of the central and neighbor crystals, respectively.
- ρ dislocation density [m^{-2}].
- E_{gb}, $E_{\rm disl}$ energy associated with grain boundaries and dislocation density, respectively.
- β, κ constants.
- $\Delta\theta$ change in angle during polygonization [deg].

[52] **Acknowledgments.** Reviews of an earlier version of the manuscript by Paul Duval and H.-R. Wenk improved this work. Discussions and editing by E. D. Waddington and C. F. Raymond are greatly appreciated, as are reviews by T. Pfeffer and a anonymous reviewer. This work was supported by grants OPP-9123660, OPP-9526707, and OPP-9815136 from the National Science Foundation.

References

Alley, R. B., Flow-law hypotheses for ice-sheet modeling, *J. Glaciol.*, *38*(129), 245–256, 1992.
Alley, R. B., J. H. Perepezko, and C. R. Bentley, Grain growth in polar ice, I, Theory, *J. Glaciol.*, *32*(112), 413–424, 1986.
Alley, R. B., A. Gow, and D. Meese, Mapping *c*-axis fabrics to study physical processes in ice, *J. Glaciol.*, *41*(137), 197–203, 1995.
Anandakrishnan, S., J. Fitzpatrick, R. B. Alley, A. Gow, and D. Meese, Shear-wave detection of asymmetric *c*-axis fabrics in the GISP2 ice core, Greenland, *J. Glaciol.*, *40*(136), 491–496, 1994.
Ashby, M. F., and P. Duval, The creep of polycrystalline ice, *Cold Reg. Sci. Technol.*, *11*(3), 285–300, 1985.
Azuma, N., A flow law for anisotropic ice and its application to ice sheets, *Earth Planet. Sci. Lett.*, *128*(3–4), 601–614, 1994.

Azuma, N., A flow law for anisotropic ice under uniaxial compressive deformation, *Cold Reg. Sci. Technol.*, *23*(2), 137–147, 1995.

Azuma, N., and K. Goto-Azuma, An anisotropic flow law for ice-sheet ice and its implications, *Ann. Glaciol.*, *23*, 202–208, 1996.

Bishop, J. F. W., and R. Hill, A theory of the plastic distortion of a polycrystalline aggregate under combined stresses, *Philos. Mag.*, *42*, 414–427, 1951.

Branger, V., M. H. Mathon, T. Baudin, and R. Penelle, "In-situ" neutron diffraction study of the cube crystallographic texture development in Fe53%-Ni alloy during recrystallization, *Scr. Mater.*, *43*(4), 325–330, 2000.

Budd, W., and T. Jacka, A review of ice rheology for ice sheet modelling, *Cold Reg. Sci. Technol.*, *16*(2), 107–144, 1989.

Castelnau, O., and P. Duval, Simulations of anisotropy and fabric development in polar ices, *Ann. Glaciol.*, *20*, 277–282, 1994.

Castelnau, O., P. Duval, R. Lebensohn, and G. R. Canova, Viscoplastic modeling of texture development in polycrystalline ice with self-consistent approach: Comparison with bound estimates, *J. Geophys. Res.*, *101*(B6), 13,851–13,868, 1996a.

Castelnau, O., T. Thorsteinsson, J. Kipfstuhl, P. Duval, and G. R. Canova, Modelling fabric development along the GRIP ice core, central Greenland, *Ann. Glaciol.*, *23*, 194–201, 1996b.

Castelnau, O., G. Canova, R. Lebensohn, and P. Duval, Modelling viscoplasctic behavior of anisotropic polycrystalline ice with a self-consistent approach, *Acta Mater.*, *45*(11), 4823–4834, 1997.

Cuffey, K. M., T. Thorsteinsson, and E. D. Waddington, A renewed argument for crystal size control of ice sheet strain rates, *J. Geophys. Res.*, *105*(B12), 27,889–27,894, 2000.

De La Chapelle, S., O. Castelnau, V. Lipenkov, and P. Duval, Dynamic recrystallization and texture development in ice as revealed by the study of deep ice cores in Antarctica and Greenland, *J. Geophys. Res.*, *103*(B3), 5091–5105, 1998.

Duval, P., Creep and fabrics of polycrystalline ice under shear and compression, *J. Glaciol.*, *27*(95), 129–140, 1981.

Duval, P., and O. Castelnau, Dynamic recrystallization of ice in polar ice sheets, *J. Phys. IV*, *5*(C3), 197–205, 1995.

Duval, P., and H. LeGac, Does the permanent creep-rate of polycrystalline ice increase with crystal size?, *J. Glaciol.*, *25*(91), 151–157, 1980.

Duval, P., and H. LeGac, Mechanical behavior of Antarctic ice, *Ann. Glaciol.*, *3*, 92–96, 1982.

Glen, J. W., The flow law of ice, in *Physics of the Movement of the Ice*, *IAHS Publ.*, *47*, 171–183, 1958.

Gödert, G., and K. Hutter, Induced anisotropy in large ice shields: Theory and its homogenization, *Continuum Mech. Thermodyn.*, *10*(5), 293–318, 1998.

Goldsby, D., and D. Kohlstedt, Creep of fine-grained ice, I, paper presented at International Symposium on the Physics and Chemistry of Ice, Int. Glaciol. Soc., Hanover, N. H., 1996.

Gow, A. J., Depth-time-temperature relationships of ice crystal growth in polar glaciers, *CRREL Res. Rep. 300*, pp. 1–19, Cold Reg. Res. and Eng. Lab., Hanover, N. H., 1971.

Gow, A. J., D. A. Meese, R. B. Alley, J. J. Fitzpatrick, S. Anandakrishnan, G. A. Woods, and B. C. Elder, Physical and structural properties of the Greenland Ice Sheet Project 2 ice core: A review, *J. Geophys. Res.*, *102*(C12), 26,559–26,575, 1997.

Guillope, M., and J. P. Poirier, Dynamic recrystallization during creep of single-crystalline halite: An experimental study, *J. Geophys. Res.*, *84*(B10), 5557–5567, 1979.

Kamb, W. B., The glide direction in ice, *J. Glaciol.*, *3*, 1097–1106, 1961.

Kamb, W. B., Experimental recrystallization of ice under stress, in *Flow and Fracture of Rocks*, *Geophys. Monogr. Ser.*, vol. 16, edited by H. Heard et al., pp. 211–241, AGU, Washington, D.C., 1972.

Kohnen, H., and A. J. Gow, Ultrasonic velocity investigations of crystal anisotropy in deep ice cores from Antarctica, *CRREL Res. Rep. 79-10*, pp. 1–18, Cold Reg. Res. and Eng. Lab., Hanover, N. H., 1979.

Kuhlmann-Wilsdorf, D., Questions you always wanted (or should have wanted) to ask about workhardening, *Mater. Res. Innovationd*, *1*(4), 265–297, 1998.

Kuhlmann-Wilsdorf, D., The theory of dislocation-based crystal plasticity, *Philos. Mag. A*, *79*(4), 955–1008, 1999.

Lebensohn, R., and C. Tome, A self consistent anisotropic approach for the simulation of plastic deformation and texture development of polycrystals: Application to zirconium alloys, *Acta Metall. Mater.*, *41*(9), 2611–2624, 1993.

Lebensohn, R., and C. Tome, A self-consistent viscoplastic model: Prediction of rolling textures of anisotropic polycrystals, *Mater. Sci. Eng. A*, *175*(1–2), 71–82, 1994.

Miguel, M.-C., A. Vespignani, S. Zapperi, J. Weiss, and J.-R. Grasso, Intermittent dislocation flow in viscoplastic deformation, *Nature*, *410*(6829), 667–671, 2001.

Mohamed, G., and B. Bacroix, Role of stored energy in static recrystallization of cold rolled copper single and multicrystals, *Acta Mater.*, *48*(13), 3295–3302, 2000.

Molinari, A., G. Canova, and S. Ahzi, A self consistent approach of the large deformation polycrystal viscoplasticity, *Acta Metall.*, *35*(12), 2983–2994, 1987.

Montagnat, M., and P. Duval, Rate controlling processes in the creep of polar ice, influence of grain boundary migration associated with recrystallization, *Earth Planet. Sci. Lett.*, *183*, 179–186, 2000.

Morland, L. W., and R. Staroszczyk, Viscous response of polar ice with evolving fabric, *Continuum Mech. Thermodyn.*, *10*(3), 135–152, 1998.

Rajmohan, N., and J. A. Szpunar, A new model for recrystallization of heavily cold-rolled aluminum using orientation-dependent stored energy, *Acta Mater.*, *48*(13), 3327–3340, 2000.

Ross, J., H. Lallemant, and N. Carter, Stress dependence of recrystallized-grain and subgrain size in olivine, *Tectonophysics*, *70*(1–2), 39–61, 1980.

Russell-Head, D., and W. Budd, Ice-sheet flow properties derived from bore-hole shear measurements combined with ice-core studies, *J. Glaciol.*, *24*(90), 117–130, 1979.

Sachs, G., Zur Ableitung einer Flie bedingung, *VDI Z.*, *72*(22), 734–736, 1928.

Sarma, G. B., and P. R. Dawson, Texture predictions using a polycrystal plasticity model incorporating neighbor interactions, *Int. J. Plast.*, *12*(8), 1023–1054, 1996.

Savage, M. K., Seismic anisotropy and mantle deformation, *Rev. Geophys.*, *37*(1), 65–106, 1999.

Shimizu, I., Stress and temperature dependence of recrystallized grain size: A subgrain misorientation model, *Geophys. Res. Lett.*, *25*(22), 4237–4240, 1998.

Shimizu, I., A stochastic model of grain size distribution during dynamic recrystallization, *Philos. Mag. A*, *79*(5), 1217–1231, 1999.

Steinemann, S., Resultats experimentaux sur la dynamique de la glace et leurs correlations avec le mouvement et la petrographie des glaciers, in *Physics of the Movement of the Ice*, *IAHS Publ.*, *47*, 184–198, 1958.

Taylor, K. C., Sonic logging at Dye 3, Greenland, M.S. thesis, pp. 1–64, Univ. of Wis., Madison, 1982.

Thorsteinsson, T., An analytical approach to deformation of anisotropic ice crystal aggregates, *J. Glaciol*., in press, 2001.

Thorsteinsson, T., J. Kipfstuhl, and H. Miller, Textures and fabrics in the GRIP ice core, *J. Geophys. Res.*, *102*(C12), 26,583–26,599, 1997.

Thorsteinsson, T., E. D. Waddington, K. C. Taylor, R. B. Alley, and D. D. Blankenship, Strain-rate enhancement at Dye 3, Greenland, *J. Glaciol.*, *45*(150), 338–345, 1999.

van der Veen, C., and I. Whillans, Flow laws for glacier ice: Comparison of numerical predictions and field measurements, *J. Glaciol.*, *36*(124), 324–339, 1990.

van der Veen, C., and I. Whillans, Development of fabric in ice, *Cold Reg. Sci. Technol.*, *22*(2), 171–195, 1994.

Wenk, H.-R., and J. M. Christie, Comments on the interpretation of deformation textures in rocks, *J. Struct. Geol.*, *13*(10), 1091–1110, 1991.

Wenk, H.-R., K. Bennett, G. Canova, and A. Molinari, Modeling plastic deformation of peridotite with the self-consistent theory, *J. Geophys. Res.*, *96*(B5), 8337–8349, 1991.

Wenk, H.-R., G. Canova, Y. Brechet, and L. Flandin, A deformation-based model for recrystallization of anisotropic materials, *Acta Mater.*, *45*(8), 3283–3296, 1997.

T. Thorsteinsson, Department of Earth and Space Sciences, University of Washington, Box 351650, Seattle, WA 98195-1310, USA. (throstho@geophys.washington.edu)